Interdisciplinary Information Sciences Vol. 15, No. 1 (2009) 91–98

ISSN 1340-9050 print/1347-6157 online
DOI 10.4036/iis.2009.91

Reducing Turn-around Times for Supernova Simulations

Katharina BENKERT[1*], Bernhard MÜLLER[2†], and Michael M. RESCH[1‡]

[1]*High Performance Computing Center Stuttgart (HLRS), University of Stuttgart, 70550 Stuttgart, Germany*
[2]*Max Planck Institute for Astrophysics, Karl-Schwarzschild-Str. 1, 85741 Garching, Germany*

Received May 29, 2008; final version accepted December 13, 2008

Many questions in the field of supernova core collapse still remain unanswered due to the complex multi-faceted nature of the problem. A direct computation of the full neutrino radiation hydrodynamics would require a sustained performance of PetaFlop/s and is therefore unfeasible on today's supercomputers. The modeling required to reduce the computational effort is accompanied by the ambiguity which physical effects are indispensable. As input parameters also contain a certain amount of uncertainty, parameter studies are necessary. For this reason, supernova simulations still require TFlop/s and a careful mapping of the software onto the given hardware is necessary to assure the maximum performance possible.

In this paper, we describe the necessary extensions to the partly existing MPI parallelization of the simulation code PROMETHEUS/VERTEX from the Max-Planck Institute for Astrophysics in Garching. With a complete distributed memory parallelization, turn-around times can be decreased substantially. We show for a 15 solar mass model that an efficient usage of up to 32 nodes NEC SX-8 is possible and therefore turn-around times can be reduced by a factor of nearly seven.

KEYWORDS: Supernovae, Radiation Hydrodynamics, Parallelization

1. Introduction

Supernovae occur in stars more massive than about eight solar masses ($M_\odot$) when nuclear fusion ceases. When the star collapses to a neutron star, a huge amount of gravitational binding energy is liberated and mostly radiated away in the form of neutrinos. They are believed, as depicted in Fig. 1, to deposit some of their energy behind the outgoing shock wave, thus powering the explosion. Despite 40 years of research, the details of this mechanism are still not completely understood due to the complex interplay of hydrodynamics, neutrino transport and nuclear physics. Today, large-scale simulations provide more and more insights into the explosion mechanism, the origin of neutron star kicks, and the production of the heavy elements.

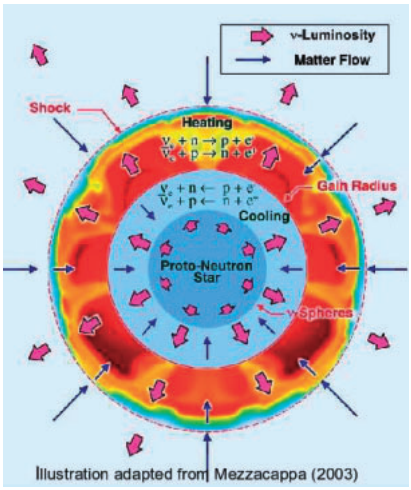

Fig. 1. Suggested mechanism.

* E-mail: benkert@hlrs.de
† E-mail: bjmuellr@mpa-garching.mpg.de
‡ E-mail: resch@hlrs.de

The full neutrino radiation hydrodynamics model with 3D hydrodynamics and a 6D neutrino transport problem would require a sustained performance of 1 to 10 PetaFlop/s, which is beyond the current capacity of modern computing facilities. Therefore, the Max-Planck Institute for Astrophysics, Garching, Germany, currently uses in their code PROMETHEUS/VERTEX a 2D hydro model and a "ray-by-ray-plus" variable Eddington factor method, respectively. Successful explosions have already been obtained for some progenitor models in the 8–15 $M_\odot$ range with this model as shown in Fig. 2. Future simulations will cover a broader range of progenitor stars, and also provide important data for nucleosynthesis studies as well as for neutrino and gravitational wave astronomy.

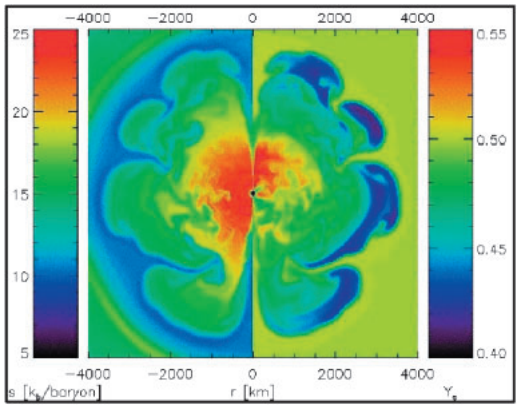

Fig. 2. Entropy and electron fraction during the explosion of an 8.8 solar mass star.

As mentioned, PROMETHEUS/VERTEX has high demands on computational power as well as main memory. This restricts the choice of suitable architectures substantially. The whole code possesses a well-scaling shared-memory parallelization using OpenMP, but only VERTEX, the resource-intensive neutrino part, has yet been parallelized using MPI. So architectures with large SMP nodes like the IBM Power4/5/6 at the computing center in Garching are one option. However, the single CPU performance is limited due to the scalar architecture. On the other hand, Müller *et al.* (2007) have shown that the code is well-suited for vector computers such as the NEC SX-8 installation at HLRS. Benkert and Fischer (2007) have recently optimized the kernel, the solution of the block-pentadiagonal linear system of equations, for this architecture. However, with only eight processors per node SX-8, the missing distributed memory parallelization of the hydrodynamics part carries more weight and limits the scalability of the code.

So far, with both options having drawbacks, the dilemma faced in all cases where high turn-around times for one single run. Since it is unlikely that further tunings would increase the single CPU performance on scalar architectures, the parallelization of the hydrodynamics part became essential being the only means to increase the overall sustained performance and thus shorten turn-around times.

The remaining paper is outlined as follows: in Section 2, the numerics of the hydrodynamic-radiation model are explained. In Section 3, the details of the parallelization including the necessary communications are presented. Results for a 15 $M_\odot$ progenitor star are presented in Section 4.

2. Numerics

The coupled system of non-linear PDEs describing the neutrino radiation hydrodynamics is decomposed via an operator splitting approach into two independent parts, a hydro(dynamic) and a neutrino-transport/interaction one. The hydrodynamics, i.e., the solution of the Euler equations for the stellar fluid consisting of nucleons, nuclei, leptons and photons, is calculated with the time-explicit finite volume code PROMETHEUS which employs the third-order Piecewise Parabolic Method (PPM) of Colella and Woodward (1984). Details on PROMETHEUS can be found in Fryxell *et al.* (1989), Keil (1997), Kifonidis (2000) and Plewa and Müller (2001). The neutrino transport part is solved with VERTEX as described in Buras *et al.* (2006) and Rampp and Janka (2002), which implements a Boltzmann solver using a "ray-by-ray plus" variable Eddington factor method. In the following, we will explain for each part the governing equations as well as their implementation in PROMETHEUS/VERTEX which is sketched in Fig. 3.

2.1 Hydrodynamics

The Eulerian, non-relativistic equations of hydrodynamics in spherical coordinates and azimuthal symmetry for an ideal fluid with mass density ρ, radial, lateral and azimuthal components of the velocity vector (v_r, v_θ, v_ϕ), specific energy $\epsilon = e + \frac{1}{2}v^2$ (e is the specific internal energy), and the gas pressure p, are given by

$$\partial_t \rho + \frac{1}{r^2}(r^2 \rho v_r) + \frac{1}{r \sin\theta}\partial_\theta(\rho \sin\theta v_\theta) = 0 \tag{1}$$

$$\partial_t(\rho v_r) + \frac{1}{r^2}\partial_r(r^2 \rho v_r v_r) + \frac{1}{r\sin\theta}\partial_\theta(\rho \sin\theta v_\theta v_r) - \rho\frac{v_\theta^2 + v_\phi^2}{r} + \partial_r p = -\rho\partial_r \Phi^{\mathrm{Newt}} + Q_{M_r} \tag{2}$$

$$\partial_t(\rho v_\theta) + \frac{1}{r^2}\partial_r(r^2 \rho v_r v_\theta) + \frac{1}{r\sin\theta}\partial_\theta(\rho \sin\theta v_\theta v_\theta) + \rho\frac{v_r v_\theta - v_\phi^2 \cot\theta}{r} + \frac{1}{r}\partial_\theta p = -\frac{\rho}{r}\partial_\theta \Phi^{\mathrm{Newt}} + Q_{M_\theta} \tag{3}$$

$$\frac{1}{r\sin\theta}\partial_\theta(\rho \sin\theta v_\theta v_\phi) + \rho\frac{v_r v_\phi + v_\theta v_\phi \cot\theta}{r} = 0 \tag{4}$$

$$\partial_t\big(\rho\varepsilon\big) + \frac{1}{r^2}\partial_r(r^2(\rho\varepsilon + p)v_r) + \frac{1}{r\sin\theta}\partial_\theta((\rho\varepsilon + p)\sin\theta v_\theta) = -\rho\left(v_r\partial_r \Phi^{\mathrm{Newt}} + \frac{v_\theta}{r}\partial_\theta \Phi^{\mathrm{Newt}}\right) + Q_E + v_r Q_{M_r} + v_\theta Q_{M_\theta}, \tag{5}$$

where Φ^{Newt} is the Newtonian gravitational potential and $\mathbf{Q}_{\mathrm{M}} = (Q_{M_r}, Q_{M_\theta})$ and Q_E are the neutrino source terms for momentum transfer and energy exchange, respectively.

As the system of equations (1)–(5) is under-determined, a closure relation is provided — the equation of state (EoS). It calculates the gas pressure p dependent on ρ, e and the chemical composition of the fluid. In the simple case, i.e., in nuclear statistical equilibrium, the composition can be described by a third variable, the electron fraction Y_e which is determined by a conservation equation

$$\partial_t(\rho Y_e) + \partial_i(\rho Y_e v_i) = Q_N, \tag{6}$$

where the source term Q_N describes the change of the net electron number density (i.e., the density of electrons minus that of positrons) due to emission and absorption of electron-flavor neutrinos. In the other case, the EoS additionally depends on the mass fractions of every nuclear species present and a similar equation to (6) must be solved for each of them.

PROMETHEUS covers steps H1 to H12 on the left side of Fig. 3. These steps form one PPM-cycle which consists of two CFL time steps H1–H6 and H7–H12. PROMETHEUS evaluates the left hand sides of the equations of hydrodynamics in a radial (r-)sweep (H2/H9) and a lateral (θ-)sweep (H4/H7). The order of r- and θ-sweep is switched after every CFL time step to restore second order convergence in time. Steps H1/H8 and H3/H10 are a result of the discretization which is discussed in Section 2.3. Since the innermost five radial zones form a single spherical core, which is a one-dimensional structure, boundary values and fluxes have to be averaged over all angular zones.

Steps H5/H11 provide the Newtonian gravitational potential Φ^{Newt} which enters on the right hand side (RHS) of the Eulerian equations (2), (3) and (5) by solving the Poisson equation

$$\Delta\Phi^{\mathrm{Newt}} = 4\pi G\rho, \tag{7}$$

where G is Newton's constant. Other contributions to the RHSs, i.e., gravitational, energy and composition changes due to neutrino and burning effects, are each calculated subsequently in operator-split steps in H6/H12.

More than one PPM-cycle c can be executed per transport time step (typically $c = 1, \ldots, 5$).

2.2 Equations for the Neutrino Transport

The neutrino distribution function $f(r, \theta, \phi, \epsilon, \Theta, \Phi, t)$ describes, at every point (r, ϕ, θ) in space, the distribution of neutrinos propagating with energy ε into direction (Φ, Θ) at time t. It influences the source terms for the energy, momentum and electron fraction of the fluid. Its evolution in time is governed by a Boltzmann equation. To make computations feasible, the seven-dimensional problem is reduced to a four-dimensional one by considering the angular moments of Θ and Φ and assuming azimuthal symmetry, i.e., independence on ϕ, as well as independence on Φ. This results in four equations: two moment equations with four unknown moments J, H, K and L to calculate the neutrino energy density J and the neutrino energy flux H. In addition, VERTEX simultaneously solves another pair of equations for the neutrino number density $\mathcal{J} = J/\epsilon$ and flux $\mathcal{H} = H/\epsilon$ in order to guarantee both energy and lepton number conservation[1]. With the Eddington factors f_K and f_L from the solution of a simplified Boltzmann equation, the higher moments $K = f_K J$ and $L = f_l J$ are computed. Additionally, two equations to conserve the neutrino number and two equations for the update of the energy e and of the electron fraction Y_e are needed. The system of moment equations in its full detail is given by Eqs. (B.13)–(B.16) in Buras *et al.* (2006).

The steps of VERTEX are displayed on the right side of Fig. 3. VERTEX solves the set of moment equations likewise in two operator-split steps corresponding to a lateral and a radial sweep. In the lateral sweep T1, the θ-dependent terms are evaluated containing derivatives of the zeroth and first order moments J and H, of $\mathcal{J}$ and of $\mathcal{H}$, which corresponds to the lateral advection of the neutrinos with the stellar fluid. This implies that equations

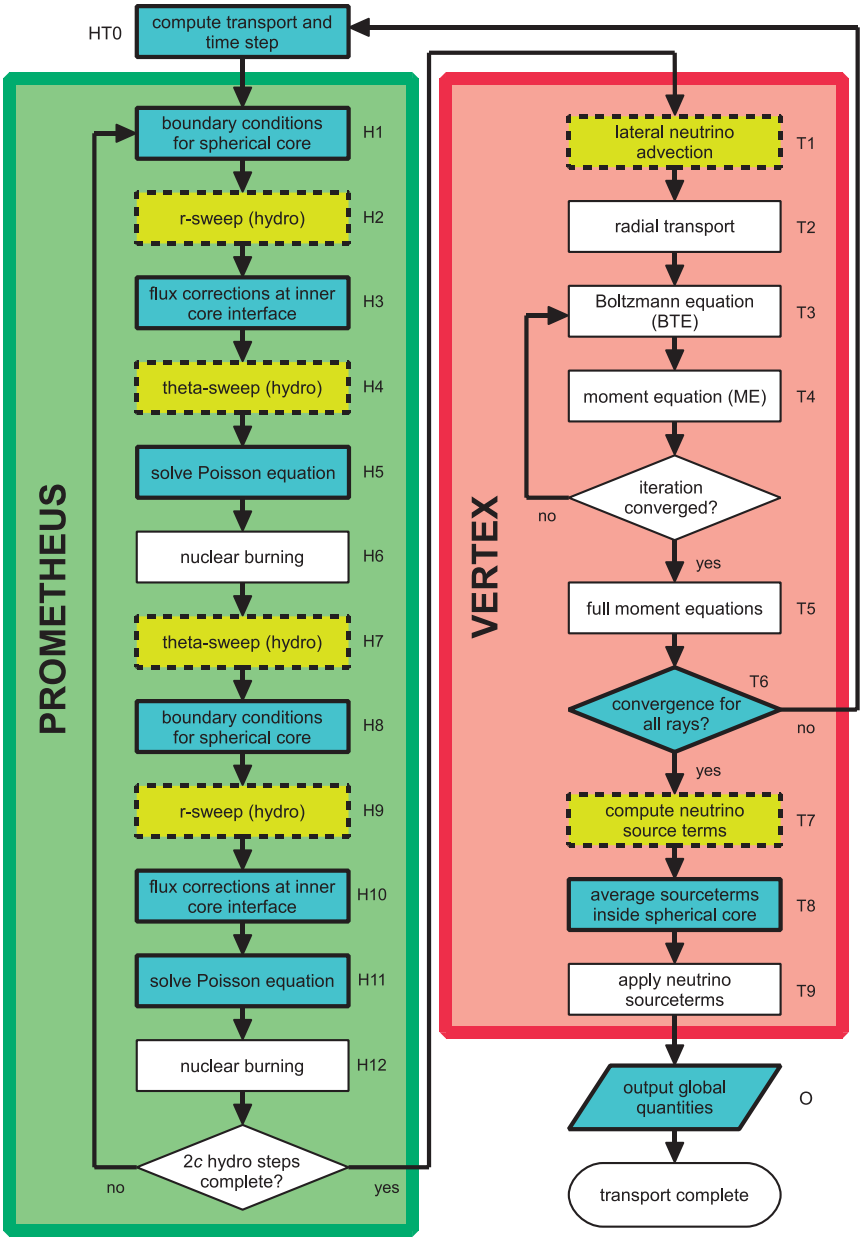

Fig. 3. Schematic overview of the algorithms of PROMETHEUS (left) and VERTEX (right). Colored boxes indicate MPI communications in the fully parallelized code (see Section 3.2) with neighborhood communications (dashed lined yellow boxes) and global communications (solid lined blue boxes).

$$\frac{1}{c}\,\partial_t \Xi + \frac{1}{r\sin\theta}\,\partial_\theta(\sin\theta\beta_\theta\,\Xi) = 0, \tag{8}$$

need to be solved with an explicit upwind scheme for each radius, each energy bin and each type of neutrino, where Ξ represents one of the moments J, H, $\mathcal{J}$ or $\mathcal{H}$.

In the radial sweep T2, the remaining θ-dependent terms are calculated. Step T3 solves the simplified Boltzmann equation for K and L. Subsequently in step T4, the moment equations for J and H are calculated, where the RHS possesses a non-local coupling in energy space due the inclusion of inelastic scattering processes. An implicit first order backward time differencing scheme is applied ray-by-ray which gives rise to independent block-pentadiagonal systems when solved with a Newton-Raphson procedure. After iterating steps T3 und T4 until convergence, the full moment equations are solved in step T5 for J, H, $\mathcal{J}$ and $\mathcal{H}$, where J and H are recalculated with higher precision.

If convergence on all rays has been obtained, the angular moments of the collision integral of the Boltzmann equation are used to calculate the source terms Q_N, Q_E and Q_{M_r} of the equations of hydrodynamics in step T7. In the ray-by-ray-plus approximation, Q_{M_θ} is given by the lateral neutrino pressure gradient. After that, the source terms are averaged inside the spherical core (T8) and applied to the hydrodynamic equations (T9).

The output of simulation results (O) completes one time step.

2.3 Discretization

The transport as well as the hydro equations are discretized on a computational domain $[0, r_{\max}] \times [\theta_{\min}, \theta_{\max}]$, basically with N_r radial zones and N_θ angular zones. For the hydrodynamic grid, the innermost five radial zones possess only one angular zone, e.g. $N_\theta = 1$. They are computed spherically as the CFL-condition would impose severe limitations on the timestep because of the singularity of the grid. For the transport grid, such modifications are not necessary as the transport equations are solved implicitly. The transport grid, however, is coarsened in radial direction outside a radius of 400–500 km since the matter becomes so thin, that neutrinos do not interact with the stellar fluid.

3. Parallelization

After describing the existing MPI parallelization, we explain the necessary steps and concepts of the MPI parallelization for the hydro part. We distinguish between next-neighbor and collective communications: in next-neighbor communications, neighboring processes according to the domain decomposition exchange data with each other in point-to-point communications. In collective operations, all processes take part simultaneously. For this application, the latter occur in two flavors: as AllReduce operations, in which an operation, e.g., a summation, is executed on a data set and the result is returned to all processes, and as AllGatherV operations, where each process sends (a varying number of) data to every other process where it is stored in rank order.

3.1 The Existing MPI Parallelization

Up to now, only the neutrino part was parallelized with MPI. The domain was decomposed over different angular zones as for the ray-by-ray Boltzmann method the neutrino moment equations decouple for different latitudes. The hydrodynamics part was redundantly executed by each process since its execution time compared to the neutrino part is short for a small number of processes. For the test case presented in Section 4, only 1.2% of the execution time of the main loop is spent in the hydro part in the serial case. The data itself was stored in Fortran common blocks and *not* distributed among the processes. During the neutrino part, each process updated its part of the data as specified by the domain decomposition. Nevertheless, all results were needed on each process to compute the hydrodynamics. As consequence, large amounts of data had to be exchanged once per time step in a collective operation (during step T6 in Fig. 3). This is a minor problem on the NEC SX-8 because of its IXS switch with transfer rates of 16 GB/s. More important is that because of the missing hydro parallelization, also some steps in the neutrino part were executed redundantly on the whole grid: the backup of transport quantities in case the transport step fails, the lateral advection of neutrinos and the mapping of transport quantities onto the hydro grid within step T7 as well as the computation of neutrino source terms (T9). As for the hydro part, these steps take only a fraction of the total computation time for a single MPI process ($< 0.6\%$ for the test case), but avoid an efficient scaling to large numbers of processes.

3.2 The Full Parallelization

The parallelization of the hydrodynamics part uses the same partitioning. Necessary parts of the code have been transformed to Fortran90 using modules with allocatable arrays. A real data distribution among the processes has been implemented. As consequence of the latter, also changes within the neutrino part were necessary and the single collective communication was replaced by multiple communications. At the moment, the MPI parallelization requires that each process covers at least four angular zones since the PPM reconstruction algorithm needs the values from four laterally adjacent cells in both directions as input for the lateral sweep. This condition is regarded insignificant for present production runs on NEC SX-8 and can be removed at any time by including communications with non-immediate neighbors if the need arises. If the domain is spread evenly across all processes, the work load is in general perfectly balanced since the amount of work per angular zone is the same. The only possibility for load imbalances to occur are different numbers of Newton iterations within step T4 or a different number of iterations needed to complete steps T3 and T4.

The following paragraphs describe the required communications within the hydrodynamics and neutrino parts. Apart from those, a collective communication (HT0) controls the multi-timestepping of the neutrino transport and determines the size of the hydro time step based on the CFL condition. At the end, two additional collective communications per global time step are necessary for data output (O).

3.2.1 Hydrodynamics

During each CFL time step, five communications take place: two next-neighbor and three collective ones of type AllReduce.

The first two collective communications result from the core discretization. As is known, the PPM method uses piecewise parabolic shape functions and therefore requires four ghost cells. During the solution of the Eulerian equations of hydrodynamics (H1/H8), the four radial zones $N_5, \ldots, N_8$ right outside the core are considered for the boundary conditions of ρ, v_i, ε, p and other values needed for the PPM method. For each variable, averages over all

corresponding angular zones are computed. The same is done during steps H3/H10 for fluxes across the inner core interface. The averaged values are needed for the single radial sweep within the core which is executed locally by every MPI process.

The third collective communication in steps H5/H11 is related to the Poison equation (7) to determine the Newtonian gravitational potential Φ^{Newt}. Using Green's method with orthonormal basis functions in spherical polar coordinates, one obtains an integral equation over r and θ. While the integration in radial direction can be executed locally, the integration in lateral direction results in a global summation.

The first next-neighbor communication serves again to provide the input for the PPM reconstruction method. During the θ-sweep (H4/H7), all the state variables in the four leftmost and rightmost angular zones covered by each process are exchanged to update the ghost-cells on the neighboring processes. The presence of the second next-neighbor communication in the radial sweeps (H2/H9) has a numerical reason: in order to avoid the phenomenon of odd-even decoupling near grid-aligned shocks investigated by Quirk (1994), PROMETHEUS adaptively switches to an approximate Riemann solver (HLLE) developed by Einfeldt (1988), which uses the values of v_θ in the adjacent grids cells in the lateral direction.

As mentioned, more than one PPM-cycle c can be executed per transport time step. Thus, one global time step would require $5 * 2 * c$ communications in the hydro part.

3.2.2 Neutrino Transport

During the neutrino transport, two next-neighbor communications and two collective ones take place.

The first communication occurs during the calculation of the neutrino transport equations (T1). As already mentioned, Eq. (8) describes the lateral advection of the neutrinos with the stellar fluid and thus couples the angular moments of the neutrino distribution of neighboring angular zones. Because of the upwind discretization scheme used, J, H, $\mathcal{J}$, $\mathcal{H}$ and $\beta_\theta = v_\theta/r$ are exchanged in a next-neighbor communication.

After one transport step, the number of iterations along with some other information are exchanged in a collective communication of type AllGatherV (T6). The purpose is to verify the convergence criteria for the radial sweep and decide whether the transport step needs to be redone.

Another next-neighbor communication is needed for the coupling between radiation and hydrodynamics (T7) when the transport grid is mapped back to the hydro grid since the momentum transfer from the neutrinos to the medium in lateral direction Q_{M_θ} is discretized with central differences. For further details, the reader is refered to Eqs. (B.16)–(B.20) in Buras *et al.* (2006). An additional collective communication is required to average the sourceterms inside the spherical core which are provided by the transport step on all processes.

4. Numerical Results

To evaluate the variants with and without parallel hydrodynamics, a $15\,M_\odot$ progenitor star with $N_r = 250$ radial and $N_\theta = 256$ angular zones was evolved for 50 time steps without a spherical core discretization. This setup is slightly smaller than for a typical production run where the number of radial zones would be twice as large. The goals of the comparison are threefold: firstly, to investigate how many processors can be used efficiently, secondly, to determine the reasons for limits imposed on parallel efficiency, and thirdly, to evaluate the consequences of the parallelization on turn-around times and thus the number of simulation runs which can now be executed in a one-year period. Since the focus of our work lies on the reduction of turn-around times and for the sake of a common pattern, we use one MPI process and eight OpenMP threads per node NEC SX-8. This allows a maximum scaling as the variant with parallel hydro requires 4 angular zones for every MPI process and multiple MPI processes per node would lower the total number of nodes that can be used. In addition, the variations between different combinations of threads and MPI processes are marginal. On one node, the differences in execution times for one thread and eight MPI processes, two threads and four MPI processes, four threads and two MPI processes as well as eight threads and one MPI process are less than 1% for the main loop.

For the variant without parallel hydrodynamics, the accumulated runtimes depicted on the left side of Fig. 4 show both an increase for the hydro and the neutrino part. For the hydrodynamics, this is clearly due to the multiple execution on each MPI process. For the neutrino part, the main reason is also the redundant execution of several steps. The parallel efficiency, also shown on the left side of Fig. 4, decreases fast to 0.91 for four nodes and to 0.82 for eight nodes. This signifies that production runs are only advisable on four nodes or less. The degree of parallelism estimated from the data is 0.967. In the 32-node run, 244.4 GB are transfered within the global communication.

Contrarily, for the variant with parallel hydrodynamics, the accumulated execution times shown on the right side of Fig. 4 increase only slightly. For the neutrino part, this results mostly from waiting times in step T6 before the AllGatherV operation to verify the convergence criteria of the neutrino transport step. For the hydro part, the increase in runtime is primarily due to the communication in step HT0. The degree of parallelism estimated from the data is now 0.997. For the 32-node run, the total amount of data communicated has been reduced to 3.2 GB. Despite this tremendous decrease of transfered data, the communication time for HT0 in the parallel version is comparable to the communication time needed to exchange all data for the variant without parallel hydrodynamics on the SX-8. For the

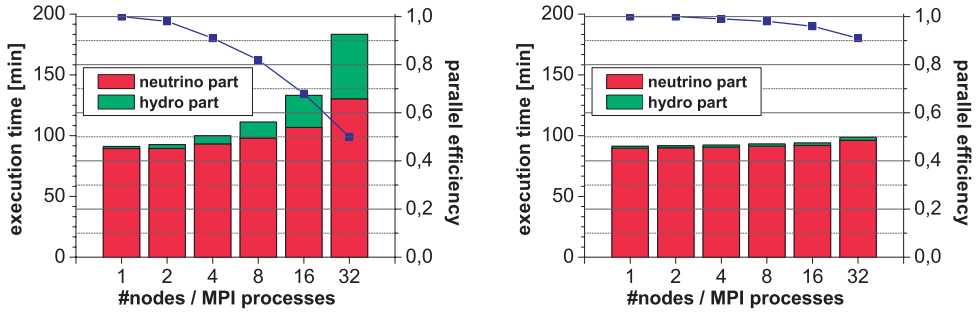

Fig. 4. Accumulated execution times for neutrino and hydro part (columns) and parallel efficiency (lines) for a $15\,M_{\odot}$ progenitor star evolved for 50 timesteps without parallel hydrodynamics (left) and with parallel hydrodynamics (right).

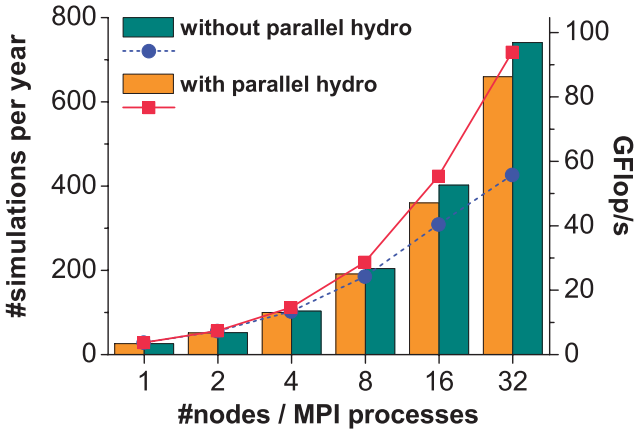

Fig. 5. Number of possible simulation runs per year (lines) and sustained performance (columns) for a $15\,M_{\odot}$ progenitor with and without parallel hydrodynamics.

parallel case, the communication in HT0 imposes a global synchronization after a larger time of calculation and is expensive due to imbalances resulting from OS jitter.

Figure 5 shows the improvements in terms of number of possible simulation runs per year and sustained performance. The former has been extrapolated from the runs with 50 timesteps including pre- and postprocessing and times for writing 1000 restart files per simulation. With an estimated 10^5 timesteps and taking into account that the application without parallel hydro scales only up to four nodes, one is able to do 103 runs with this particular grid setup (on four nodes) without parallel hydro and nearly seven times as much, namely 718 (on 32 nodes) at best.

5. Conclusion

In this paper, we have shown that the MPI parallelization of the hydrodynamics part in addition to the existing distributed memory parallelization of the neutrino part is the second important step towards TFlop performance for the neutrino hydrodynamics simulation code PROMETHEUS/VERTEX after adapting its kernel to the vector architecture. The measurements on the NEC SX-8 installation at HLRS show that the weak scaling has improved greatly, allowing an efficient use of up to 32 nodes in contrast to four nodes beforehand. With this achievement, nearly seven times as much simulation runs can be done which eases parameter studies on input parameters and physical modeling.

Our future research will focus on the performance of a more detailed progenitor star with improved physics. The Adaptive Data and Communication Library (ADCL), developed at the University of Houston and HLRS, will be integrated into the code as a means to optimize the performance of MPI communications in a self-adaptive way. Is is anticipated that a different algorithm for the collective communications will further enhance the parallel performance.

Notes

[1]This procedure is necessary because a conservative discretization of the neutrino energy equation does not necessarily conserve lepton number despite the fact that the neutrino energy and number density equations are *analytically* equivalent.

REFERENCES

[1] Benkert, K., and Fischer, R., An efficient implementation of the Thomas-Algorithm for block penta-diagonal systems on vector computers, In Shi, Y., van Albada, G., Dongarra, J., and Sloot, P., (Eds.), Computational Science—ICCS 2007, LNCS 4487, pp. 114–151, Springer (2007).

[2] Buras, R., Rampp, M., Janka, H.-T., and Kifonidis, K., "Two-dimensional hydrodynamic core-collapse supernova simulations with spectral neutrino transport," *A & A*, **447**: 1049–1092 (2006).

[3] Colella, P., and Woodward, P. R., "The piecewise parabolic method (PPM) for gas dynamical simulations," *J. Comp. Phys.*, **54**: 174–201 (1984).

[4] Einfeldt, B., "On Godunov-type methods for gas dynamics," *SIAM J. Numer. Anal.*, **25**: 294–318 (1988).

[5] Fryxell, B., Müller, E., and Arnett, W., Hydrodynamics and nuclear burning, preprint, MPA-449, Max Planck Institute for Astrophysics, Garching (1989).

[6] Keil, W., Konvektive Instabilitäten in entstehenden Neutronensternen, PhD thesis, Technische Universität München (1997).

[7] Kifonidis, K., Nucleosynthesis and hydrodynamic instabilities in core collapse supernovae, PhD thesis, Technische Universität München (2000).

[8] Müller, B., Marek, A., Benkert, K., Kifonidis, K., and Janka, H.-T., Supernova simulations with the radiation hydrodynamics code PROMETHEUS/VERTEX, In Resch, M., Roller, S., Lammers, P., Furui, T., Galle, M., and Bez, W., (Eds.), High Performance Computing on Vector Systems 2007, pp. 195–210, Springer (2007).

[9] Plewa, T., and Müller, E., AMRA: "An Adaptive Mesh Refinement hydrodynamic code for Astrophysics," *Comput. Phys. Commun.*, **138**: 101–127 (2001).

[10] Quirk, J. J., "The piecewise parabolic method (PPM) for gas dynamical simulations," *Int. J. Num. Meth. Fluids*, **18**: 555 (1994).

[11] Rampp, M., and Janka, H.-T., "Radiation hydrodynamics with neutrinos," *A & A*, **396**: 361–392 (2002).